

Computational Techniques for Simulating Natural Convection in Three-Dimensional Enclosures with Tetrahedral Finite Elements

K. O. Ladipo R. Glowinski T.W. Pan

Abstract

This article discusses computational techniques for simulating natural convection in three-dimensional domains using finite element methods with tetrahedral elements. These techniques form a new numerical procedure for this kind of problems. In this procedure, the treatment of advection by a *wave equation approach* is extended to three-dimensional unstructured meshes with tetrahedra.

Numerical results of natural convection of an incompressible Newtonian fluid in a cubical enclosure at Rayleigh numbers in the range 10^3 to 10^6 are obtained and they are in good agreement with those in literature obtained by other methods.

key words Three-dimensional domains, Finite element methods, Tetrahedral elements, Natural convection, Incompressible fluids.

§1 Introduction

Simulation of natural convection flows in three-dimensional geometries has been an area of active research in recent years. In the past decade, most researchers who performed calculations in three-dimensional geometries were hindered from applying sufficient resolutions, by limitations on computer storage. For example, Mallinson

and De Vahl Davis in [1, 1977] used a very coarse mesh with up to 15^3 nodes, Pepper D.W. in [2, 1987] applied only $33 \times 17 \times 9$ nodes. More recently, with the availability of more powerful computers, researchers are now able to perform calculations on meshes with better resolutions. Le Peutrec and Lauriat [3, 1990] used mesh with up to 41^3 nodes, Fusegi *et al.* in [4, 1991] used meshes with up to 62^3 nodes. Janssen *et al.* in [5, 1993] reported results with 120^3 nodes mesh, but they generated the results by symmetry, after performing actual simulation with only one-fourths of this number. Natural convection is governed by a coupled system of Navier-Stokes equations and energy equations.

The objective of this paper is to present a finite element method for simulating natural convection of an incompressible fluid in three-dimensional geometries using tetrahedral elements with unstructured mesh. An operator-splitting scheme of Marchuk-Yanenko is applied to split the coupled system into three sub-problems namely, the pressure, transport and diffusion sub-problems. This decouples the difficulties usually associated with non-linearity and incompressibility constraint. The pressure and diffusion sub-problems are time discretized by backward-Euler-type method. The non-linear advection is treated by a *wave equation approach*. Space discretization is achieved by a finite element method where pressure, velocity and temperature are approximated by continuous piecewise-linear polynomials on meshes consisting of 4-node tetrahedral elements. The mesh for velocity and temperature is twice finer than the pressure mesh so that the *inf-sup* condition is satisfied. A systematic method of constructing these velocity-pressure meshes, such that each pressure tetrahedral element is a *macro-element* consisting of eight sub-tetrahedra for velocity, is discussed in this article. We extend the two-dimensional method for constructing a pressure macro-element, by connecting edge mid-points, to three dimensional meshes. The numerical procedure presented in this article also extends the treatment of advection

by a *wave equation approach* in [6], [7] to three-dimensions while combining other different numerical techniques and thus forming a new, efficient, solution procedure suitable for simulating motion of an incompressible fluid in three-dimensional geometries with unstructured meshes.

Results obtained for the numerical example of natural convection of air in a cubical box, illustrate the accuracy and reliability of this new procedure. The three-dimensional results also validate the usual assumptions in two-dimensional simulations and elucidates three-dimensional effects on this flow phenomenon.

§2 Governing Equations for Natural Convection

We consider natural convection of an incompressible viscous Newtonian fluid enclosed in a three-dimensional rectangular domain, $\Omega \subset \mathbf{R}^3$, with boundary denoted by Γ . The geometry and coordinate system for the enclosure are shown in Figure 1. The natural convection is induced by the non-zero temperature gradient between the two vertical surfaces, Γ_l (at $x = 0$) and Γ_r (at $x = L_x$). The remaining four surfaces, $(\Gamma \setminus \Gamma_l \cup \Gamma_r)$ are assumed to be perfectly thermally insulated.

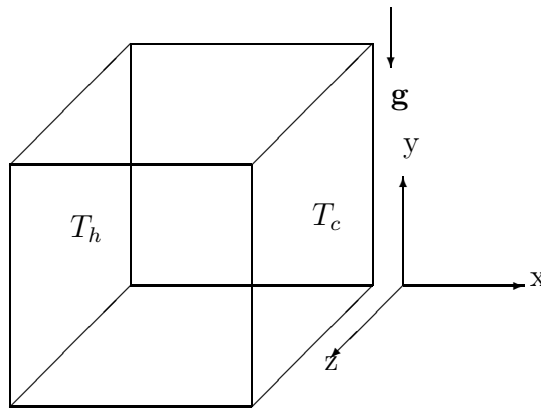


Figure 1: Geometry and coordinate system for cubical enclosures,

$$(0 \leq x \leq L_x ; 0 \leq y \leq L_y ; 0 \leq z \leq L_z).$$

With the Boussinesq approximation, the vector form of the dimensionless governing equations in a finite time interval $(0, t^N)$ are:

$$\frac{\partial \mathbf{u}}{\partial t} + (\mathbf{u} \cdot \nabla) \mathbf{u} - Pr \Delta \mathbf{u} + \nabla p = Ra Pr \theta \hat{j} \quad \text{in } \Omega \times (0, t^N), \quad (1)$$

$$\frac{\partial \theta}{\partial t} + (\mathbf{u} \cdot \nabla) \theta - \Delta \theta = 0 \quad \text{in } \Omega \times (0, t^N), \quad (2)$$

$$\nabla \cdot \mathbf{u} = 0 \quad \text{in } \Omega \times (0, t^N), \quad (3)$$

where ,

$$Ra = \frac{g\beta(T_h - T_c)L_x^3}{\nu\alpha}, \quad \text{the Rayleigh number,} \quad (4)$$

$$Pr = \frac{\nu}{\alpha}, \quad \text{the Prandtl number,} \quad (5)$$

$\mathbf{u}(x, y, z, t) = \{u_i\}_{i=1}^3 = (u_x, u_y, u_z)$ is the flow velocity,

t is elapsed time, $(\mathbf{u} \cdot \nabla) \mathbf{u}$ is a symbolic notation for the non-linear vector term

$$\left\{ \sum_{j=1}^3 u_j \frac{\partial u_i}{\partial x_j} \right\}_{i=1}^3,$$

$$\{x_i\}_{i=1}^3 = (x, y, z),$$

$\theta(x, y, z, t)$ is the temperature,

$p(x, y, z, t)$ is the pressure ,

β is the coefficient of thermal expansion of the fluid,

α is the coefficient of thermal diffusivity of the fluid,

ν is the kinematic viscosity coefficient of the fluid,

\mathbf{g} is the gravitational acceleration.

This set of dimensionless equations is subject to the following *initial and boundary*

conditions:

$$\left\{ \begin{array}{l} 1\mathbf{u}(x, y, z, 0) = \mathbf{0} \quad \text{in } \Omega, \\ \theta(x, y, z, 0) = 0 \quad \text{in } \Omega, \\ \mathbf{u}(x, y, z, t) = \mathbf{0} \quad \text{on } \Gamma \times (0, t^N), \\ \theta(x, y, z, t) = 1 \quad \text{on } \Gamma_\ell \times (0, t^N), \\ \theta(x, y, z, t) = 0 \quad \text{on } \Gamma_r \times (0, t^N), \\ \frac{\partial \theta}{\partial \bar{n}}(x, y, z, t) = 0 \quad \text{on } \Gamma \setminus (\Gamma_\ell \cup \Gamma_r) \times (0, t^N). \end{array} \right. \quad (6)$$

In order to obtain the dimensionless equations, the distance between the colder and hotter surfaces, L_x , has been chosen as the reference length and the scale factors for velocity, time and pressure are chosen as, α/L_x , L_x^2/α , $\rho_0\alpha^2/L_x^2$ respectively. The dimensionless temperature is defined as $\theta = \frac{T - T_c}{T_h - T_c}$.

Thus, the three-dimensional rectangular model domain has dimensions $A_x \times A_y \times A_z$ where A_{x_i} is the *aspect ratio* in the x_i direction.

§3 Time Discretization by Marchuk-Yanenko-Type Operator Splitting Method of Problem Equations(1) - (6)

Let $\Delta t > 0$ be the time step and $t^n = n\Delta t$. At every time interval $[t^n, t^{n+1}]$, the Marchuk-Yanenko-type operator-splitting method involves a sequence of computations as follows:

$$(I) \quad \mathbf{u}^0 = \mathbf{u}_0 ; \theta^0 = \theta_0, \quad (7)$$

then, for $n \geq 0$, \mathbf{u}^n, θ^n given, we compute $(\theta^{n+1/3}, \mathbf{u}^{n+1/3}, p^{n+1})$, $(\theta^{n+2/3}, \mathbf{u}^{n+2/3})$ and $(\theta^{n+1}, \mathbf{u}^{n+1})$ as follows:

(II) Solve the *pressure sub-problems*:

$$\begin{cases} \theta^{n+1/3} = \theta^n & \text{in } \Omega, \\ \frac{\mathbf{u}^{n+1/3} - \mathbf{u}^n}{\Delta t} = -\nabla p^{n+1} & \text{in } \Omega, \\ \mathbf{u}^{n+1/3} = \mathbf{0} & \text{on } \Gamma, \\ \nabla \cdot \mathbf{u}^{n+1/3} = 0 & \text{in } \Omega, \end{cases} \quad (8)$$

(III) then solve the *transport sub-problems*:

$$\begin{cases} \frac{\partial \theta}{\partial t} + \mathbf{u}^{n+1/3} \cdot \nabla \theta = 0 & \text{in } \Omega \times (t^n, t^{n+1}), \\ \frac{\partial \mathbf{u}}{\partial t} + \mathbf{u}^{n+1/3} \cdot \nabla \mathbf{u} = \mathbf{0} & \text{in } \Omega \times (t^n, t^{n+1}), \\ \mathbf{u}(t^n) = \mathbf{u}^{n+1/3}, \quad \theta(t^n) = \theta^{n+1/3}. \end{cases} \quad (9)$$

$$\text{Set } \mathbf{u}^{n+2/3} = \mathbf{u}(t^{n+1}), \quad \theta^{n+2/3} = \theta(t^{n+1}). \quad (10)$$

(IV) Finally, solve the *diffusion sub-problems*:

$$\begin{cases} \frac{\theta^{n+1} - \theta^{n+2/3}}{\Delta t} - \Delta \theta^{n+1} = 0 & \text{in } \Omega, \\ \theta^{n+1} = 1 & \text{on } \Gamma_\ell, \\ \theta^{n+1} = 0 & \text{on } \Gamma_r, \\ \frac{\partial \theta^{n+1}}{\partial n} = 0 & \text{on } \Gamma \setminus (\Gamma_\ell \cup \Gamma_r), \\ \frac{\mathbf{u}^{n+1} - \mathbf{u}^{n+2/3}}{\Delta t} - Pr \Delta \mathbf{u}^{n+1} = Ra Pr \theta^{n+1} \hat{\mathbf{j}} & \text{in } \Omega, \\ \mathbf{u}^{n+1} = \mathbf{0} & \text{on } \Gamma. \end{cases} \quad (11)$$

§4 On the Finite Element Approximation of sub-problems (8) - (11)

The entire domain $\Omega = \Omega_h$, constituting the computational domain, is discretized into a finite set, \mathcal{T}_h , of tetrahedra inside which velocity, pressure and temperature are continuous and the collection of the tetrahedra satisfies the following properties:

1. $T_h = \overline{T_h} \subset \overline{\Omega_h}$ for all $T_h \in \mathcal{T}_h$.

2. $\mathcal{T}_h = \{T_h\}$ is finite.
3. For $T_1, T_2 \in \mathcal{T}_h$, if $\text{interior}(T_1) \neq \text{interior}(T_2)$, then only one of the following is possible:
 - $T_1 \cap T_2 =$ a vertex common to T_1 and T_2 or,
 - $T_1 \cap T_2 =$ a common edge or face of T_1 and T_2 or,
 - $T_1 \cap T_2 = \emptyset$.
4. $\bigcup_{T_h \in \mathcal{T}_h} T_h = \overline{\Omega}_h$.

The finite element mesh for pressure is twice coarser than the mesh for velocity. The mesh for temperature is the same as that for velocity. Let \mathcal{T}_h be the finite collection of the tetrahedra for velocity and \mathcal{T}_{2h} , a similar collection for pressure. Piecewise-linear approximation is employed for all variables including pressure. Hence, the vertices of the tetrahedra in \mathcal{T}_h and \mathcal{T}_{2h} form the *nodes* for the finite element meshes for velocity, temperature and pressure respectively.

A new method of discretizing Ω_h and Ω_{2h} into 4-node tetrahedral elements, such that the pressure tetrahedra are macro-elements consisting of eight sub-tetrahedra, is presented in this report. This is achieved by first discretizing the domain into a finite set of 8-cornered *brick-like* macros, each of which is then split into two prisms along a vertical mid-plane through a diagonal line on the top face and through the center of gravity of the *brick-like* macro. Each of the two prisms is then divided into 3 tetrahedra in a very unique way. \mathcal{T}_{2h} is constructed first and, as in two-dimensional cases, \mathcal{T}_h is constructed from \mathcal{T}_{2h} by connecting the edge midpoints on the faces and on any resulting vertical mid-plane. A detailed explanation of the steps involved in this *tetrahedralization* is given in the appendix. We however make the following remarks here:

§5 Remarks

1. The six generic tetrahedral elements have different shapes but the same volume which is one-sixth of the volume of the particular *brick-like* macro containing them.
2. In order for each pressure tetrahedral element to properly contain exactly eight sub-tetrahedra, after the edge-midpoints have been connected, it is necessary that, one set of three tetrahedra on one prism must be a reflection of the second set of three tetrahedra on the other prism about the vertical plane through the diagonal of the *brick-like* macro.
3. Although, a method, for splitting a *brick-like* macro into six tetrahedra was given, by Zienkiewicz, in [8], the discussion did not include the situation of multi-level grids as in this present case.

§6 Discrete sub-problems and Weak Formulations

Weak formulation of each set of sub-problems, determined by the operator-splitting, are obtained using the following fundamental discrete spaces:

$$V_h = \{v_h \mid v_h \in C^0(\overline{\Omega}_h), v_h|_T \in \mathcal{P}_1, \forall T \in \mathcal{T}_h\}, \quad (12)$$

$$V_{0h} = \{v_h \mid v_h \in V_h, v_h|_\Gamma = 0\}, \quad (13)$$

$$\Pi_{0h} = \{\phi_h \mid \phi_h \in V_h, \phi_h|_{\Gamma_\ell \cup \Gamma_r} = 0\}, \quad (14)$$

$$P_h = \left\{ q_h \mid q_h \in C^0(\overline{\Omega}_{2h}), q_h|_T \in \mathcal{P}_1, \forall T \in \mathcal{T}_{2h}, \int_{\Omega_{2h}} q_h d\Omega = 0 \right\}. \quad (15)$$

In equations(12) - (15), \mathcal{P}_1 is the space of polynomials in three variables of degree ≤ 1 . The discrete approximation associated to the finite element spaces described

above, for the weak formulation of the pressure sub-problems is:

Find $\{\mathbf{u}_h^{n+1/3}, p_h^{n+1}\} \in (V_{0h})^3 \times P_h$ such that,

$$\frac{1}{\Delta t} \int_{\Omega_h} u_i^{n+1/3} v_h d\Omega = \int_{\Omega_h} p_h^{n+1} \frac{\partial v_h}{\partial x_i} d\Omega + \frac{1}{\Delta t} \int_{\Omega_h} u_i^n v_h d\Omega \quad \forall v_h \in V_{0h}, \quad (16)$$

for each component of $\mathbf{u}_h = \{u_i\}_{i=1}^3$,

$$\int_{\Omega_{2h}} q_h \nabla \cdot \mathbf{u}_h^{n+1/3} d\Omega = 0, \quad \forall q_h \in P_h, \quad (17)$$

$$\mathbf{u}_h^{n+1/3} = \mathbf{0}, \quad \text{on } \Gamma. \quad (18)$$

The transport sub-problems combined with the wave equation approach described in [6] and [7] give a set of semi-discrete sub-problems with weak formulation given as:

Find $\theta_h \in V_h$ and $\mathbf{u}_h \in (V_{0h})^3, \forall t \in [t^n, t^{n+1}]$ such that,

$$\int_{\Omega_h} \left(\frac{\partial^2 \theta_h}{\partial t^2} \right) \phi_h d\Omega + \int_{\Omega_h} \left(\mathbf{u}_h^{n+1/3} \cdot \nabla \phi_h \right) \left(\mathbf{u}_h^{n+1/3} \cdot \nabla \theta_h \right) d\Omega = 0, \quad \forall \phi_h \in V_h, \quad (19)$$

$$\int_{\Omega_h} \left(\frac{\partial^2 \mathbf{u}_h}{\partial t^2} \right) \cdot \mathbf{w}_h d\Omega + \int_{\Omega_h} \left(\mathbf{u}_h^{n+1/3} \cdot \nabla \mathbf{w}_h \right) \left(\mathbf{u}_h^{n+1/3} \cdot \nabla \mathbf{u}_h \right) d\Omega = 0, \quad \forall \mathbf{w}_h \in (V_h)^3, \quad (20)$$

$$\theta_h(t^n) = \theta_h^{n+1/3}, \quad \mathbf{u}_h(t^n) = \mathbf{u}_h^{n+1/3}, \quad (21)$$

$$\theta(t) = \begin{cases} 1 & \text{on } \Gamma_\ell, \\ 0 & \text{on } \Gamma_r \end{cases} \quad (22)$$

The solution of a wave-like equation such as eq.(19) and eq.(20) has been described in [6] and [7] for uniformly structured meshes. It involves time discretizing the equation by a second-order finite difference scheme with an initialization step consisting of solution of full discrete version of eq.(9). It is noteworthy to mention that since the discrete wave-like equations are explicit there is no need to store any square matrix thereby, conserving computer memory. However, a local time step $\Delta t/Q$ has to be chosen with integer Q sufficiently large so that the CFL condition is not violated.

The set eq.(11), of diffusion subproblems is approximated by the following discrete sub-problems:

Find $\theta_h^{n+1} \in V_h$ and $\mathbf{u}_h^{n+1} \in (V_{0h})^3$, such that,

$$\int_{\Omega_h} \left(\frac{\theta_h^{n+1} - \theta_h^{n+2/3}}{\Delta t} \right) \phi_h d\Omega + \int_{\Omega_h} \nabla \theta_h^{n+1} \cdot \nabla \phi_h d\Omega = 0, \quad \forall \phi_h \in \Pi_{0h}, \quad (23)$$

$$\theta_h^{n+1} = \begin{cases} 0 & \text{on } \Gamma_r, \\ 1 & \text{on } \Gamma_\ell, \end{cases} \quad (24)$$

$$\begin{aligned} \int_{\Omega_h} \left(\frac{\mathbf{u}_h^{n+1} - \mathbf{u}_h^{n+2/3}}{\Delta t} \right) \cdot \mathbf{w}_h d\Omega + Pr \int_{\Omega_h} \nabla \mathbf{u}_h^{n+1} \cdot \nabla \mathbf{w}_h d\Omega \\ = RaPr \int_{\Omega_h} \theta_h^{n+1} \hat{j} \cdot \mathbf{w}_h d\Omega, \quad \forall \mathbf{w}_h \in (V_h)^3, \end{aligned} \quad (25)$$

§7 Solution Strategy for the Pressure Subproblems (16) - (18)

Let $\mathbf{x} = (x, y, z)$ and $\{\omega_m(\mathbf{x})\}_{m=1}^{N_h}$ be the vector basis for V_h such that,

$$\omega_m(\mathbf{x}_\ell) = \begin{cases} 1 & \text{if } \mathbf{x}_\ell = \mathbf{x}_m \\ 0 & \text{if } \mathbf{x}_\ell \neq \mathbf{x}_m \end{cases} \quad (26)$$

for each node on the velocity mesh. After applying Galerkin method on the discrete weak formulation we get the following discrete sub-problem at each node \mathbf{x}_m on the velocity mesh:

Find $\{\mathbf{u}_h^{n+1/3}, p_h^{n+1}\} \in (V_{0h})^3 \times P_h$ such that,

$$\frac{1}{\Delta t} \int_{\Omega_h} u_i^{n+1/3} \omega_m d\Omega = \int_{\Omega_h} p_h^{n+1} \frac{\partial \omega_m}{\partial x_i} d\Omega + \frac{1}{\Delta t} \int_{\Omega_h} u_i^n \omega_m d\Omega, \quad (1 \leq i \leq 3) \quad (27)$$

$$\mathbf{u}_h^{n+1/3} = \mathbf{0}, \quad \text{on } \Gamma, \quad (28)$$

$$\int_{\Omega_{2h}} \omega_k \nabla \cdot \mathbf{u}_h^{n+1/3} d\Omega = 0, \quad \text{at each node } \mathbf{x}_k \text{ on the pressure mesh.} \quad (29)$$

This sub-problems is solved by a preconditioned conjugate gradient (PCG) algorithm described in [6] and [7]. Proper evaluation of some integrals in the PCG algorithm is very crucial to the overall performance of this numerical technique. These include

integrals of the forms $\int_{\Omega_h} p_h^{n+1} \frac{\partial \omega_m}{\partial x_i} d\Omega$ and $\int_{\Omega_{2h}} \omega_k \nabla \cdot \mathbf{u}_h^{n+1/3} d\Omega$ which involve product of discrete functions over coarse and fine meshes. The following is a summary of the techniques applied to these integrals:

1. All integrals of the form $\int_{\Omega} fg d\Omega$ are approximated by the trapezoidal method globally on the element domain.
2. All integrals of the form $\int_{\Omega_h} p_h \frac{\partial \omega_m}{\partial x_i} d\Omega$ are computed on the fine velocity mesh element-by-element. On each pressure element, the function p_h is interpolated linearly along element edges. Also, over each velocity element, p_h is approximated by the average of its nodal values on the vertices.
3. The integrals of the form $\int_{\Omega_{2h}} \omega_k \nabla \cdot \mathbf{u}_h d\Omega$ are computed over the coarse pressure mesh element-by-element. In each pressure tetrahedral element, the nodal values of the coarse-mesh basis function ω_k on the vertices of each of the 8 included velocity elements are obtained by linear interpolation along the edges. $\nabla \cdot \mathbf{u}_h$ is piecewise-constant over each velocity element since \mathbf{u}_h is approximated by a piecewise-linear function.

The PCG steps include the solution of a Neumann problem with solution belonging to the space of functions with mean-value zero. Since this problem is solved on a relatively coarser mesh, with banded storage, it is expected that memory requirement will be a manageable size on most modern computers. Thus the Neumann problem is solved by direct method after cholesky factorization as suggested by Glowinski in [9, page 267]. However, since its solution has mean-value zero the following steps must be performed together with the direct method:

1. Set one of the unknowns to zero and delete the corresponding row and column; The $N \times N$ linear system in ϕ (say) will reduce to $(N - 1) \times (N - 1)$ linear system in ϕ' ,

2. Solve the reduced linear system by direct method, for ϕ' ,
3. compute mean value of $\phi' = \frac{1}{meas(\Omega)} \int \phi' d\Omega$,
4. Set $\phi = \phi' - (\text{mean value of } \phi')$. ($\int \phi d\Omega$ must be zero or in practice $\int \phi d\Omega \leq \varepsilon$).

§8 Solution Strategy for the Diffusion Subproblems (23) and (25)

The integrals in eq.(23) and eq.(25) are assembled over all the fine-mesh tetrahedral elements. With proper ordering of nodes, the diffusion sub-problems for temperature and velocity components result in linear systems of nodal values of the form

$$\mathbf{Ax} = \mathbf{f} \tag{30}$$

where \mathbf{A} is a symmetric positive definite, banded, sparse matrix. The bandwidth of \mathbf{A} , however grows very rapidly as the resolution is increased, so that memory requirement becomes prohibitively large even on supercomputers, despite banded storage. Thus it is more practicable to solve these linear systems for temperature and velocity components by iterative methods. A careful observation reveals that with piecewise-linear approximations, \mathbf{A} has only 15 non-zero diagonals in each case. Since it is also symmetric, a substantial amount of memory is freed by storing only the main diagonal and the 7 non-zero upper (or lower) diagonals.

The associated Dirichlet boundary condition should be enforced in a manner that preserves the symmetry and sparse nature of \mathbf{A} . A method of achieving this is discussed by Stasa in [10, pp 59-61]. The diffusion linear systems of the form eq.(30) are solved by conjugate gradient algorithm of Hestenes and Steifels (CGHS) given for example in [11]. This algorithm involves matrix-vector multiplications which are performed within the bandwidth and in a manner that prevents “*fill-ins*”. Only 7 multiplication

operations are required per row. To accelerate and ensure convergence, preconditioning is usually necessary. A way to achieve this is to ensure that Gerschgorin disks for the iterates are concentric by performing *symmetric scaling*, where the main diagonal elements are scaled to unity before commencing the iteration process. The linear system for temperature is solved first. Its converged value is applied to solve the system for the velocity components. Further, since the three linear systems for the segregated velocity components are independent, they are solved concurrently at each iteration step of CGHS algorithm. After scaling, the number of iterations required for convergence of CGHS algorithm is usually a minute fraction of the size of the linear system. For example, on a 41^3 velocity mesh the CGHS algorithm for the linear system for temperature converged in 29 to 41 iterations depending on the value of Ra . On the same mesh, the CGHS algorithm for the linear system for the segregated velocity components converged in 37 iterations.

§9 A numerical Example

The numerical techniques presented in this report have been applied to simulate natural convection in a cubical enclosure containing air with prandtl number 0.71 at Ra in the range 10^3 to 10^6 . Initially, the enclosed fluid is stationary and the uniform temperature in the enclosure and its boundaries is T_c °C. Later, the surface Γ_ℓ is heated uniformly to a temperature T_h °C while the temperature on the surface Γ_r is held fixed at T_c °C. These two surfaces are maintained at these temperatures thereafter while the remaining four surfaces of the cube are considered to be perfectly thermally insulated. The resulting density variation within the confined fluid is assumed to be small enough that the Boussinesq approximation is valid.

§10 Results and Discussion

Steady state results were obtained for the numerical example on unstructured meshes with 41^3 and 45^3 velocity nodes. Steady state solution is assumed when

$$\frac{\|u_i^{new} - u_i^{old}\|_2}{\|u_i^{new}\|_2} \leq \varepsilon, \quad (31)$$

where u_i is one of the velocity components and ε is taken as 10^{-5} .

Mesh of up to 41^3 velocity nodes was used for $Ra = 10^3$ and 10^4 with $\Delta t = 1/4000$. For $Ra = 10^5$ and 10^6 , when the boundary layer is relatively thinner, non-uniform mesh of 45^3 velocity nodes was used with $\Delta t = 1/9000$. The time increment in the re-discretization of the transport sub-problems was taken in each case as $\tau = \frac{\Delta t}{10}$. The construction on the non-uniform mesh, where $13/16$ is taken as estimate for the boundary layer thickness, is summarized in Table 1.

$Ra = 10^5$ and 10^6	sub-interval	No of divisions (coarse mesh)
45^3 fine mesh	$0 \leq x, y, z \leq 3/16$	5
	$3/16 \leq x, y, z \leq 13/16$	12
	$13/16 \leq x, y, z \leq 1$	5

Table 1: Construction of non-uniform meshes in cubical enclosure.

Computations were performed on DEC Alpha PW500au, a single processor, virtual memory machine and a linux desk-top with 512MB core memory. Computations for each Ra were started from the initial conditions given in equation(6). A mesh with 41^3 velocity nodes requires 70MB of memory while a mesh with 45^3 velocity nodes requires 99MB of memory. An iteration in time, consisting of solution of the pressure, transport and diffusion subproblems, takes average of 1.64 minutes of CPU time. The PCG algorithm converged in 7 to 8 iterations after initial transients.

The *Nusselt number*, a measure of the dimensionless heat transfer rate across the isothermal walls, was computed on the hot wall ($x = 0$), in terms of the *overall*

Nusselt number, \overline{Nu} and *y-averaged Nusselt number*, $Nu_{av}(z)$, defined by the following equations:

$$\overline{Nu} = - \int_{z=0}^{z=A_z} \int_{y=0}^{y=A_y} \left. \frac{\partial \theta}{\partial x} \right|_{x=0} dy dz. \quad (32)$$

$$Nu_{av} = - \int_{y=0}^{y=A_y} \left. \frac{\partial \theta}{\partial x} \right|_{x=0} dy. \quad (33)$$

For the cubical enclosure $A_y = 1.0$ and $A_z = 1.0$ The local heat flux $\partial\theta/\partial x$, was approximated by a second order forward-difference formula and the integrals were evaluated using the trapezoidal rule.

Variations of all variables with respect to z were investigated at each of the Rayleigh numbers applied. These variations in the z -direction are however weaker in magnitude than in other directions. In Figure 6 and Figure 7 the distributions of $(u_y)_{max}(z)$ at $x = 0.5$ and the *y-averaged Nusselt number*, $Nu_{av}(z)$, are illustrated at each Rayleigh number.

§11 Validation

A comparison of the values of \overline{Nu} and the *mean Nusselt number* $Nu_{av}(0.5)$ with results of Fusegi *et al.* [4] at each of the Rayleigh numbers used is given in Table 2. The results obtained using this present numerical procedure are in good agreement with those of Fusegi *et al.*. Also, in agreement with Fusegi *et al.* [4], Janssen *et al.* [5] and Mallinson *et al.* [1], at $Ra = 10^5$ and 10^6 , the z -variations of $Nu_{av}(z)$ are apparent near the end walls ($z = 0$ and $z = 1$), where it increases sharply. Janssen *et al.* [5] also reported a value of 0.2585 for $\overline{Nu}Ra^{-1/4}$ at $Ra = 10^6$. That is, \overline{Nu} is 8.6396 at this Rayleigh number and this represents a difference of only 0.27% of the value obtained using this present numerical procedure (See Table 3).

Ra	Quantity	Wave Equation	Fusegi <i>et al.</i> [4]	% Error
10^3	\overline{Nu}	1.2466	1.085	12.96 %
	$Nu_{av}(0.5)$	1.2563	1.105	12.04%
10^4	\overline{Nu}	1.9737	2.10	- 6.4%
	$Nu_{av}(0.5)$	2.1461	2.302	- 7.26%
10^5	\overline{Nu}	4.2055	4.361	- 3.70%
	$Nu_{av}(0.5)$	4.497	4.464	0.73%
10^6	\overline{Nu}	8.6628	8.770	- 1.24%
	$Nu_{av}(0.5)$	8.8434	9.012	- 1.91 %

Table 2: Comparison of Nusselt numbers with results of Fusegi *et al.*

Ra	Quantity	Wave Equation	Janssen <i>et al.</i> [5]	% Error
10^6	$\overline{Nu}Ra^{-1/4}$		0.2585	
	\overline{Nu}	8.6628	8.6396	0.27%

Table 3: Comparison of Nusselt numbers with results of Janssen *et al.*

In agreement with Janssen *et al.* [5], at $Ra = 10^5$ and 10^6 , $(u_y)_{max}(z)$ has two sharp peaks close to the lateral walls. At $Ra = 10^5$, the peaks occur at $(0.075, 0.5, 0.15)$ and $(0.075, 0.5, 0.85)$. At $Ra = 10^6$, the peaks occur at $(0.0375, 0.5, 0.0937)$ and $(0.0375, 0.5, 0.9625)$. The value and location of the z -direction local maximum in each case are given in Table 4.

	z -direction local maximum	Location at $y = 0.5$
$Ra = 10^5$	89.442	$x = 0.075, z = 0.15$
$Ra = 10^6$	314.1738	$x = 0.0375, z = 0.0937$

Table 4: Comparison of the peaks for $(u_y)_{max}(z)$ with results of Janssen *et al.*

The transverse variations of characteristic quantities, were further investigated. From the mesh plots of velocity components, temperature and pressure on the yz -plane at $x = 0.5$ (not shown, see ref. [6]), it was observed that for a generic variable f , representing u_x , u_y , θ or p , the following relation holds:

$$f(x, y, z) \approx f(x, y, 1 - z) \quad \forall x, y, z. \quad (34)$$

u_z on the other hand satisfies the relation,

$$u_z(x, y, z) \approx -u_z(x, y, 1 - z) \quad \forall x, y, z. \quad (35)$$

This symmetry property is sometimes imposed by researchers in order to reduce calculations to only half of the entire computational domain.

Also, from the contour plots on xy -plane (at $z = 0.5$) and mesh plots on xz -plane (at $y = 0.5$) (ref. [6]), it was observed that there is also a special type of symmetry about the line $(0.5, 0.5, z)$ (that is, the line $y = 0.5$ on yz -plane at $x = 0.5$), through the center of gravity, so that the following relations are satisfied:

$$u_x(x, y, z) \approx -u_x(1 - x, 1 - y, z), \quad (36)$$

$$u_y(x, y, z) \approx -u_y(1 - x, 1 - y, z), \quad (37)$$

$$u_z(x, y, z) \approx +u_z(1 - x, 1 - y, z), \quad (38)$$

$$p(x, y, z) \approx +p(1 - x, 1 - y, z), \quad (39)$$

$$\theta(x, y, z) \approx 1 - \theta(1 - x, 1 - y, z). \quad (40)$$

These two spatial symmetries have been observed by Janssen *et al.* [5] and they exploited it by performing actual computations over only a quarter of the entire cubical enclosure.

References

- [1] Mallinson, G. D. and De Vahl Davis, G., Three-Dimensional Natural Convection in a Box: A Numerical Study , *J. of Fluid Mech.*, 1977:, **83**:, pp. 1 - 31.
- [2] Pepper, D. W., Modeling of Three-Dimensional Natural Convection with a Time-Split Finite-Element Technique, *Numerical Heat Transfer*, 1987, **vol. 11**, pp. 31 - 35.
- [3] Le Peutrec, Y. and Lauriat,G., Effects of Heat Transfer at Side Walls on Natural Convection in Cavities, *Int. J. Heat Mass Transfer*, **112**, pp 370-378, 1990.
- [4] Fusegi, T., Hyun, J. M., Kuwahara, K. and Farouk, B., A Numerical Study of Three-Dimensional Natural Convection in a Differentially Heated Cubical Enclosure, *Int. J. Heat Mass Transfer*, **vol. 34, no 6**, pp 1543 - 1557, 1991.
- [5] Janssen, R. J. A., Henkes, R. A. W. M., Hoogendoorn, C. J., Transition to Time-Periodicity of a Natural-Convection Flow in a 3D Differentially Heated Cavity, *Int. J. Heat Mass Transfer*, **vol. 36, no 11**, pp 2927 - 2940, 1993.
- [6] Ladipo K.O., A wave Equation Approach to Numerical Simulation of Natural Convection in Rectangular Enclosures, *Ph.D. Thesis, University of Houston*, , 2002.
- [7] Pan T. W., Glowinski, R., A Projection/Wave-like Equation method for the numerical simulation of Incompressible Viscous Fluid Flow Modeled by The

Navier-Stokes Equations, *Computational Fluid Dynamics Journal*, 2000, **vol. 9, no 2**, pp. 28-42.

- [8] Zienkiewicz, O. C., The Finite Element Method, Third Edition, *McGraw-Hill(UK)*, **London**, 1977.
- [9] Glowinski, R., Finite Element Methods for the Numerical Simulation of Incompressible Viscous Flow, *Lectures in Applied Mathematics, AMS, Providence, Rhode Island*, **vol. 28**, 1991.
- [10] Stasa, Frank L., Applied Finite Element Analysis for Engineers, *Harcourt Brace Jovanovich Publishers*, **U.S.A.**, 1985.
- [11] Jennings, Alan and McKeown, J. J., Matrix Computation, second edition, *John Wiley & Sons, Ltd.*, **Chichester, England**, 1992.

Appendix

A A Systematic Method of Discretizing A Three-Dimensional Domain into Four-Node Tetrahedral Elements

Let \sum_h and \sum_{2h} be the set of all nodes on Ω_h and Ω_{2h} respectively. The first step in the domain discretization is the construction of \mathcal{T}_{2h} which is illustrated by the following steps:

- Divide the three dimensional domain into *brick-like macros*,

$$\bigcup_{j=1}^{N_{2h}} \{(x, y, z) | x_j \leq x \leq x_j + \Delta x; y_j \leq y \leq y_j + \Delta y; z_j \leq z \leq z_j + \Delta z\}, \quad (41)$$

where $N_{2h} = \text{card}(\sum_{2h})$.

A typical *brick-like* macro, with corners labeled A, B, C, D, E, F, G, H, is shown in Figure 2. Point A has coordinate (x_j, y_j, z_j) .

- Divide each *brick-like* macro into two prisms - one with corners H, E, B, C, D, A and the other prism with corners H, E, F, B, C, G along diagonals $\{\overline{HC}, \overline{EB}\}$ or $\{\overline{DG}, \overline{AF}\}$ (see Figure 3).
- Sub-divide the first prism into three tetrahedra, through line segments $\{\overline{DE}, \overline{DB}, \overline{HB}\}$.
(*top vertex-to-bottom edge construction*)
- Sub-divide the second prism into three tetrahedra, through line segments $\{\overline{FH}, \overline{FC}, \overline{HB}\}$.
(*bottom edge-to-top vertex construction*)

Thus, each 8-cornered *brick-like* macro on the coarser mesh is divided into six tetrahedral elements for pressure.

Observe that the three tetrahedral elements on the first prism may be obtained from those on second prism by reflecting first prism about the line segment, \overline{HC} . Thus, we may reverse the order of connecting points between these two prisms. That is, we may sub-divide the first prism into three tetrahedra through line segments $\{\overline{AH}, \overline{AC}, \overline{HB}\}$ (*bottom edge-to-top vertex construction*). The second prism must correspondingly be sub-divided into three tetrahedra through line segments $\{\overline{GE}, \overline{GB}, \overline{HB}\}$ (*top vertex-to-bottom edge construction*). We may also use diagonal \overline{EC} in place of \overline{HB} . If this reflection property is taken into consideration, any appropriate combination of line segments, as described above, will produce the identical set of six tetrahedral elements. This method of discretizing a brick-like macro into six tetrahedra is unique in the sense that, the six tetrahedra are generic elements for all the tetrahedral elements in \mathcal{T}_{2h} and \mathcal{T}_h . The six generic tetrahedra are shown in Figure 4.

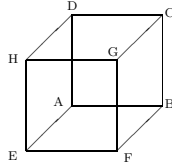


Figure 2: A typical *brick-like* macro.

The finite set \mathcal{T}_h for velocity is next constructed from \mathcal{T}_{2h} by connecting the edge-midpoints on the faces of each tetrahedron and on any resulting vertical mid-plane following the steps for constructing the six generic tetrahedra itemized above.

Thus, each pressure tetrahedral element is sub-divided into eight smaller tetrahedra, each of which is similar in shape to one of the six generic tetrahedra depicted in Figure 4.

Typical set of 8 velocity elements in two generic pressure macro-elements are delineated in Figure 5.

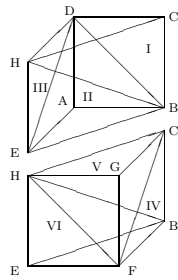


Figure 3: A systematic division of a *brick-like* macro into six tetrahedra.

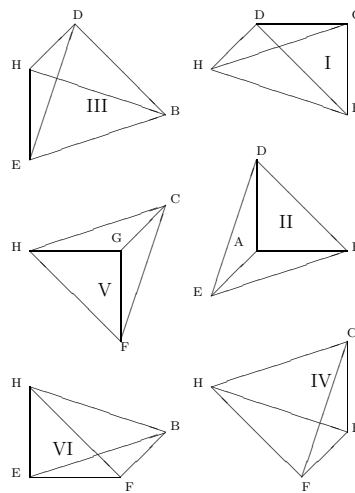


Figure 4: The six generic tetrahedral elements.

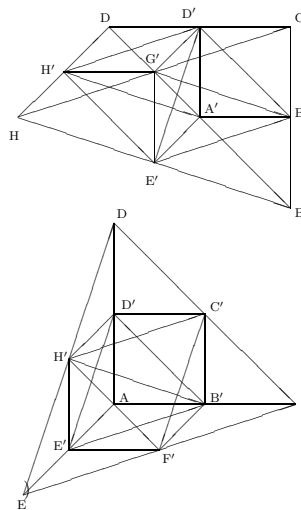


Figure 5: Typical pressure macro-elements with 8 sub-tetrahedral.

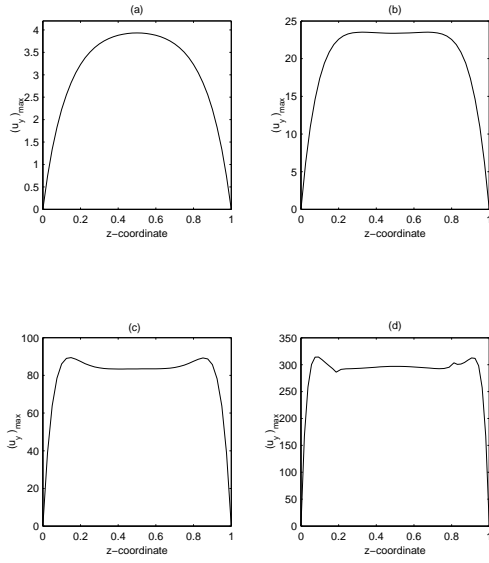


Figure 6: Distribution of $(u_y)_{max}$ along z -axis in the cubical enclosure at (a) $Ra = 10^3$ (b) $Ra = 10^4$ (c) $Ra = 10^5$ and (d) $Ra = 10^6$.

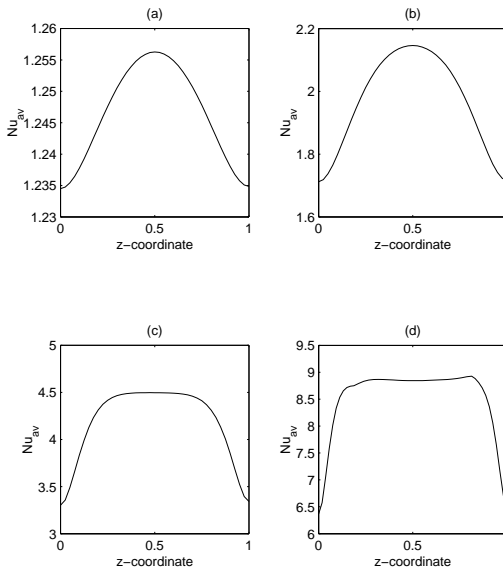


Figure 7: Distribution of y -averaged Nusselt number along z -axis in the cubical enclosure at (a) $Ra = 10^3$ (b) $Ra = 10^4$ (c) $Ra = 10^5$ and (d) $Ra = 10^6$.